Cold sintering and electric characterization of ZnO-$BaTiO_3$ composites

*L. Coutinho[1], R. G. Aredes[1], E. Antonelli[1]**

[1]Universidade Federal de São Paulo, Science and Technology Institute, Advanced Ceramic Laboratory, 12231-280, S. José dos Campos, SP, Brazil

Abstract

The sintering is an essential step in the processing of ceramics materials. A number of researchers have reported new techniques for sintering. However, in general, the process still demands high temperatures. This paper reports the results of the cold sintering of ZnO-$BaTiO_3$ composites. The microstructural, structural, and electric properties of the composite were studied. We obtained high densities (>95%) for pure ZnO and for the composition with 10 wt% of $BaTiO_3$ at a low temperature of sintering (250 °C/1 h). The increase of $BaTiO_3$ content reduced the grain size and degraded the sinterability of ZnO. The crystalline structure was investigated by X-ray diffraction and confirmed the separation of the phases after the cold sintering. The $BaTiO_3$ added in the composite reduced the values of conductivity, permittivity, and also the dielectric loss.

Keywords: ceramics, cold sintering, impedance spectroscopy, dielectrics.

INTRODUCTION

Sintering is a process in which particles are consolidated into compact solid materials, with mechanical resistance, through a diffusion process typically mediated by thermal energy [1]. Due to the high melting temperatures for ceramic materials, conventional sintering is commonly performed at high temperatures. For many oxide materials, the sintering temperature is above 1000 °C, which consumes energy and generally requires sophisticated experimental apparatus [1, 2]. Previous studies have documented strategies for sintering ceramics at low temperatures, as reactive hydrothermal liquid-phase sintering [3, 4], room temperature densification [5], and hydrothermal hot pressing [6]. Recently, researchers have proposed a new methodology for the sintering of ceramic compounds called the cold sintering process (CSP) [2, 7-11]. These authors obtained dense ceramics at low temperatures of ~250 °C. For the cold sintering, a small volume fraction of a liquid phase is added to the starting powders. Mechanical and chemical effects kinetically improve mass transport while densification follows under uniaxial pressure. The densification occurs by a combination of dissolution, precipitation, and nucleation [7-11]. An effectively sintered material has primary bonds between the particles (covalent, ionic, metallic, or a mixture of them) [4]. Under dry conditions, these primary bonds are generally obtained at high temperatures. However, they can even be obtained at lower temperatures when environmental parameters such as pressure or a liquid are present in the process [2, 4]. It has been noted that the formation of a supersaturated liquid is fundamental for CSP. The solubility of the powder in the liquid used in CSP is typically obtained by partial solubilization of particles [4]. However, it can be achieved by the addition of different chemical groups [6]. The mechanisms operating during CSP are not limited to the dissolution and reprecipitation process. The presence of the liquid facilitates the rotation and rearrangement of grains under pressure and increase the initial density of the compact [2]. Besides, it has been reported the formation of secondary phases and lattice disorder on the powder surface [4, 6].

Previous studies have reported the cold sintering of ZnO [7, 10, 12]. These works described high densities for ZnO in a single step of heat treatment. It has been demonstrated that some densification was possible with only water (pH 7) as a liquid agent [10]. However, the addition of acetic acid to the aqueous solution increases the densities and changes the microstructure of CSP ZnO ceramics [10, 12]. Recent evidence suggests that during CSP the grain boundaries and interfaces of ZnO present high defect chemistry due to the ions absorption resulting in higher surface energy [12]. This mechanism reduces the activation energy of atomic diffusion and promotes the sintering of ZnO during the CSP [12]. Cold sintering of $BaTiO_3$ has been reported by some authors [2, 13, 14]. Ma et al. [14] obtained relative densities of 96.8% and a grain size of 122 nm for cold sintering at 180 °C. However, these densities were achieved after the heat treatment at 900 °C. These authors had used as a liquid medium for sintering 1 molar solution of $Ba(OH)_2$. The other works found for sintering $BaTiO_3$ were published by Guo et al. [2, 11, 13]. These authors also obtained high densities only after a post-heat treatment at 900 °C. Recently, Tsuji et al. [15] have demonstrated the CSP of $BaTiO_3$ in a single step at 300 °C; the sintering was performed under a uniaxial pressure of 520 MPa for 12 h using a molten hydroxide flux.

Composite materials are defined as the mixing of two or more materials without chemical reactions between the phases [16]. These classes of materials combine unusual properties that are not achievable by conventional materials. However, little attention has been paid to the study and characterization of electroceramic composites (ceramic/ceramic) [17]. The high temperatures required to sinter ceramics make it difficult to obtain ceramic composites once

*https://orcid.org/0000-0001-5029-1115

these temperatures allow the diffusion between the ions. Additions of small fractions of ZnO to $BaTiO_3$ ceramics as a dopant are traditionally reported to increase the density and decrease the sintering temperatures [18, 19]. Wang et al. [20] have recently reported the synthesis of $BaTiO_3$/ZnO composite ceramics obtained by the conventional solid-state method and that the composite induces a temperature-stable dielectric permittivity. Slimani et al. [21] studied the impact of ZnO addition on dielectric properties of $BaTiO_3$ ceramics for radiofrequency and microwave applications. It has been shown that the introduction of $BaTiO_3$ in the ZnO matrix increases the dielectric constant of the composite and decrease the dielectric loss [22]. This work aimed to obtain dense ceramic composites of ZnO-$BaTiO_3$ using the cold sintering technique and to study the microstructural, structural, and electrical properties of this composite. In particular, we were interested in combining ZnO's excellent sinterability with the dielectric properties of $BaTiO_3$.

EXPERIMENTAL

The $BaTiO_3$ (BT) powder was prepared through the conventional ceramic method, starting from high-purity precursor powders of $BaCO_3$ (Vetec, 99%) and TiO_2 (Alfa, 99%). The precursor powders were ball milled (MA500, Marconi) for 12 h in a polypropylene bottle with zirconia balls (2 mm in diameter) and isopropyl alcohol. The powder was dried at 85 °C in an autoclave and calcined at 1200 °C/2 h (BT). The calcined BT powder was mixed with the ZnO powder (Neon, 99.8%) in the mass proportion of x= 1, 0.9, 0.8, 0.5, and 0.1 for xZnO-(1-x)BT, hereafter named ZnO, 90ZnO-10BT, 80ZnO-20BT, 50ZnO-50BT, and 10ZnO-90BT, respectively. These powders were also ball milled for 6 h in polypropylene bottles with zirconia balls (2 mm in diameter) and isopropyl alcohol and also dried at 85 °C. To provide the liquid phase during the cold sintering process (CSP), a solution of acetic acid and distilled water (1 $mol.L^{-1}$) was added to powders (100 $\mu L.g^{-1}$). The powders and liquid were mixed and then ground in an agate mortar for 10 min. The mixture was transferred directly to the die (15 mm of diameter) used in CSP. The CSP was conducted under a conventional uniaxial hydraulic press (MPH10, Marcon) with a heated die of steel. We used a type of jacket heater with a mica band that allowed temperatures higher than 350 °C. The temperature was controlled by a thermocouple positioned inside the die, close to the powder cavity (5 mm). Ceramics bodies were cold sintered under the pressure of 166 MPa at 250 °C/1 h and a heating rate of 5 °C/min.

The particle size analysis was performed using the laser diffraction technique (mod. 1090, Cilas). The measurements were based on the Fraunhofer scattering theory and an obscuration index of 12% was used. The final density of the sintered ceramics was determined by the geometrical method, based on the samples' mass and volume. These data, together with the calculated theoretical density (ρ_{theo}) from the rule of mixtures [23], were used to find out the final relative densities. Both crystalline phases and microstructural developments were followed by X-ray diffraction (XRD, Ultima IV, Rigaku), with monochromatic CuKα radiation (λ=1.5406 Å), and scanning electron microscopy (SEM, Inspec 500, FEI), respectively. The grain size was evaluated by the intercept method [24] directly on the SEM images of fractured surfaces of the ceramics. The microscope was coupled with energy-dispersive X-ray spectroscopy (EDS), allowing the evaluation of the Ti atomic distribution in the composites. The electrical measurements, in terms of impedance (Z*=Z'+jZ"), were carried out at room temperature using an impedance/gain-phase analyzer (SI 1260, Solartron) in the frequency range of f= 10 Hz to 1 MHz. Electric contacts consisted of silver paste previously applied on both parallel faces of the pellets and diffused at 150 °C for 1 h.

RESULTS AND DISCUSSION

Fig. 1a presents the cumulative volume as a function of the equivalent particle diameter of $BaTiO_3$ (BT), ZnO (as received), and 90ZnO-10BT that was milled for 6 h. The D50 (median diameter) values for the samples were 0.39±0.01, 13.54±0.35, and 6.95±0.10 μm for BT, ZnO, and 90ZnO-10BT, respectively. The 90ZnO-10BT equivalent particle size showed a reduction of ~50% after 6 h of milling as compared with the pure, not milled ZnO. Fig. 1b presents the particle size distribution curves (incremental volume) and an SEM micrograph of 90ZnO-10BT powder. The ZnO particles showed an inhomogeneous size distribution, typical of agglomerated systems. In particular, the distribution curves revealed a modal particle size at ~0.32 μm in the mixture, which was confirmed by the SEM characterization.

Fig. 2a presents the density and grain size behavior as a function of the composite composition. We obtained a high density for pure ZnO (98%±2%) that was in accordance with the fracture micrograph (Fig. 2b). This micrograph reveals a well-sintered sample and homogeneous grain growth of hexagonal geometry (0.9±0.5 μm). We attributed the unconformity of equivalent particle size (Fig. 1a) with the grain size of sintered ceramics to the tendency of the agglomeration of ZnO particles. The introduction of 10 wt% of BT in ZnO decreased the density (94%±2%) and the grain size (0.4±0.2 μm). Besides, the sintered microstructure did not incorporate the BT particles that are viewed in Fig. 2c as isolated particles (white grains). With 20 wt% of BT, the composite's cold sinterability was drastically reduced, and the density was only 76%±2%. We observed that the grain size was ~0.35 μm for higher contents of BT. With 50% of BT, the microstructure was typical of green consolidated ceramic bodies and the cold sintering did not effectively promote mass transport. Fig. 2e presents an EDS compositional image for 50ZnO-50BT where the Ti elemental mapping was represented as blue points. We observed a homogeneous distribution of Ti atoms that can be extended for $BaTiO_3$ distribution. The rapid density reduction together with the grain size reduction are indications that BT reduced the cold sinterability of ZnO ceramic. Some authors tend to

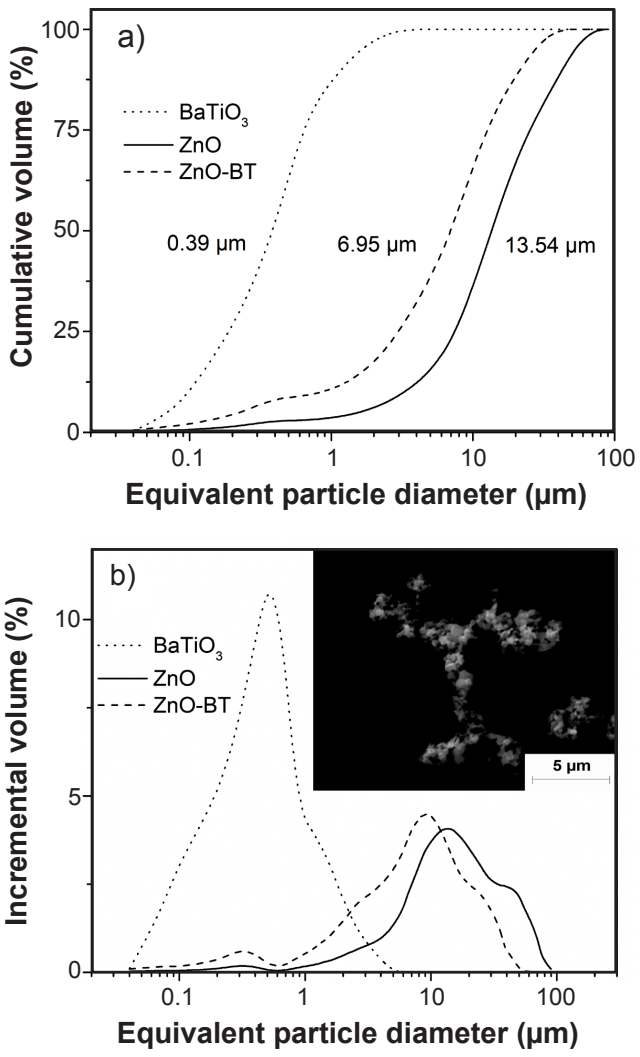

Figure 1: Cumulative volume (a) and incremental volume (b) as a function of equivalent particle diameter for powders of BT, 90ZnO-10BT, and ZnO.

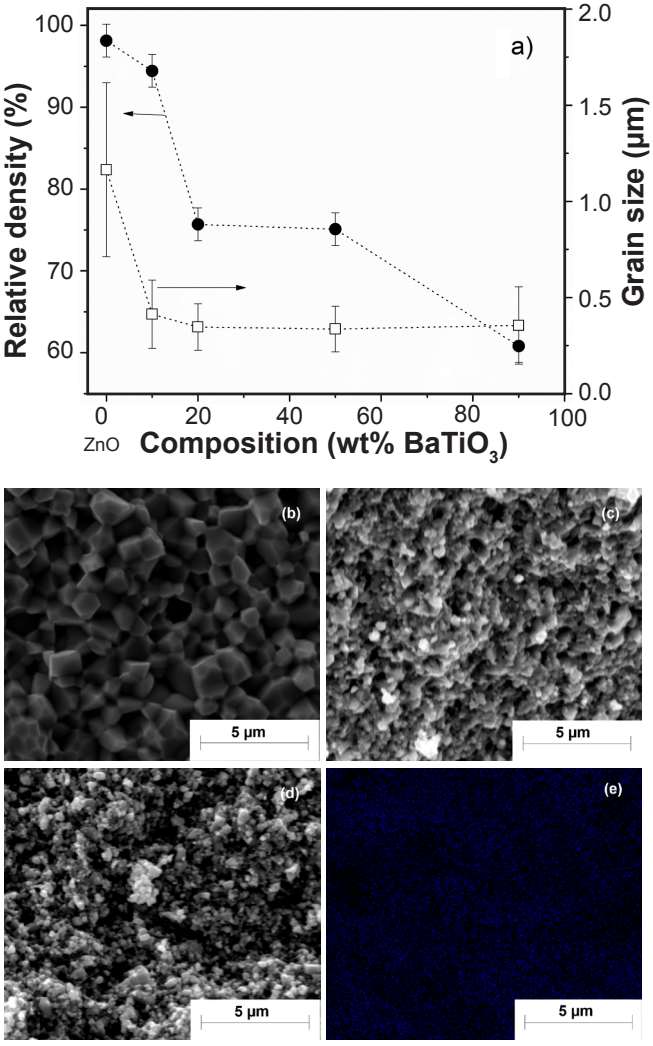

Figure 2: Relative density and grain size as a function of composite composition (a), SEM micrographs for ZnO (b), 10ZnO-90BT (c), and 50ZnO-50BT (d) ceramics, and the EDS elemental mapping image for Ti distribution in 50ZnO-50BT ceramic (e).

separate the cold sintering into a two-stage process. In stage I, the compaction occurs by uniaxial mechanical force with enhanced lubricity between particles due to the liquid, and in stage II, the temperature is elevated under constant pressure and the solubility is enhanced [6, 7]. During stage I, ~60% of density is expected for the compacted powder [12]. The low density result for 10ZnO-90BT indicated that the cold sintering process (CSP) of this composition was limited to stage I and presented characteristics of a well-compacted powder. Finally, it should be recognized that the limit for cold sintering of these composites with high densities is 10 wt% of BT added to ZnO, at least for the experimental conditions reported here.

Fig. 3 shows the XRD patterns for the pure ZnO and ZnO-BT cold sintered ceramics (250 °C/1 h). The ZnO phase was indexed as a trigonal structure (ICSD 290322) and the BT phase as a tetragonal perovskite structure (ICSD 259052). BT samples produced by CSP are reported to present a cubic structure [6]. As expected, we identified in Fig. 3 only the tetragonal structure for BT, once micrometric particles were applied. We observed the phase separation for all sintered samples that confirmed the ceramic composite formation. Fig. 3b evidences this phase separation in the peaks observed at 31.6° (BT) and 31.8° (ZnO), which became separated for all compositions. Besides, the increase of BT content resulted in an intensity decrease of the peak at 36.3° (ZnO) while the peak at 39.0° (BT) had its intensity increased. ZnO is naturally a hygroscopic material and has the characteristic of presenting some dissolution in water [12]. This dissolution process is improved with the acidification of water using acetic acid [10] or by using/forming zinc acetate [12]. Here, this process did not result in detectable second phases (Fig. 3).

Fig. 4 presents the AC conductivity (σ_{ac}) for ZnO-BT composites. The Jonscher's power law for dielectric responses explains the σ_{ac} observed for the composite [25]:

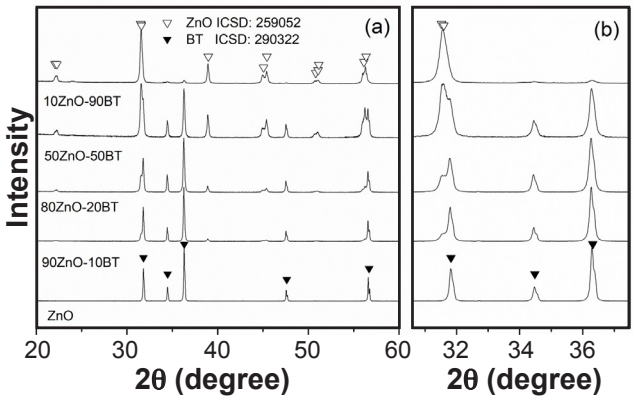

Figure 3: XRD patterns of the cold sintered ZnO ceramic and ZnO-BT composites.

$$\sigma_{ac} = \sigma_{dc} + A.\ \omega^{n} \qquad (A)$$

where σ_{dc} is DC bulk conductivity, A is a thermal activated constant, and n represents the degree of ion interaction with the lattice. Accordingly, observe in Fig. 4 that for low frequencies, the σ_{ac} was almost independent of frequency and this contribution was related to the σ_{dc} conductivity. The inverses of σ_{dc} conductivity values were taken (ρ_{dc}) and are presented in Table I. The resistivity increased with the introduction of BT in composites, and the behavior was nonlinear. It should be noted that all the curves at high frequencies fit almost the same conductivity (Fig. 4). Previous studies of CSP identified DC conductivity values in the range of 10^{-4} to 10^{-6} S/cm for ZnO ceramics [10, 12, 26]. These conductivity values are close to those observed in Fig. 4; however, they are low when compared to conventionally sintered ZnO (~10 S/cm) [27]. It was reported that the increase of ZnO conductivity in CSP is obtained after heat treatment in Ar atmosphere [26]; the authors related this effect to the increase of crystallinity and desorption of oxygen on the grain boundaries that enhance the presence of oxygen vacancies.

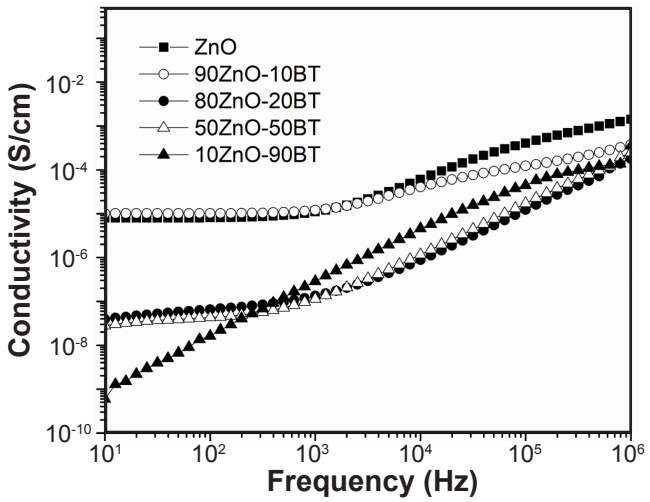

Figure 4: AC conductivity (σ_{ac}) versus frequency for ZnO and composites of ZnO-BT.

Table I - Dielectric permittivity at 1 kHz (ε'), permittivity corrected using Eq. B (ε^{PF}), dielectric loss (tanδ), and DC resistivity (ρ_{dc}).

Sample	ε'	ε^{PF}	tanδ	ρ_{dc} (Ω.cm)
ZnO	8505	8942	2.18	$1.25x10^{5}$
90ZnO-10BT	7082	7727	3.13	$1.02x10^{5}$
80ZnO-20BT	128.6	207.4	1.37	$2.52x10^{7}$
50ZnO-50BT	115.5	184.3	0.98	$3.53x10^{7}$
10ZnO-90BT	50.9	123.4	0.04	$1.67x10^{9}$

Fig. 5 presents the room temperature dielectric constant (ε') and dielectric loss (tanδ) properties of ZnO-BT composites over a frequency range from 10 Hz to 1 MHz. The dielectric constant and dielectric loss decreased quickly with the increase of BT content at low frequencies. This

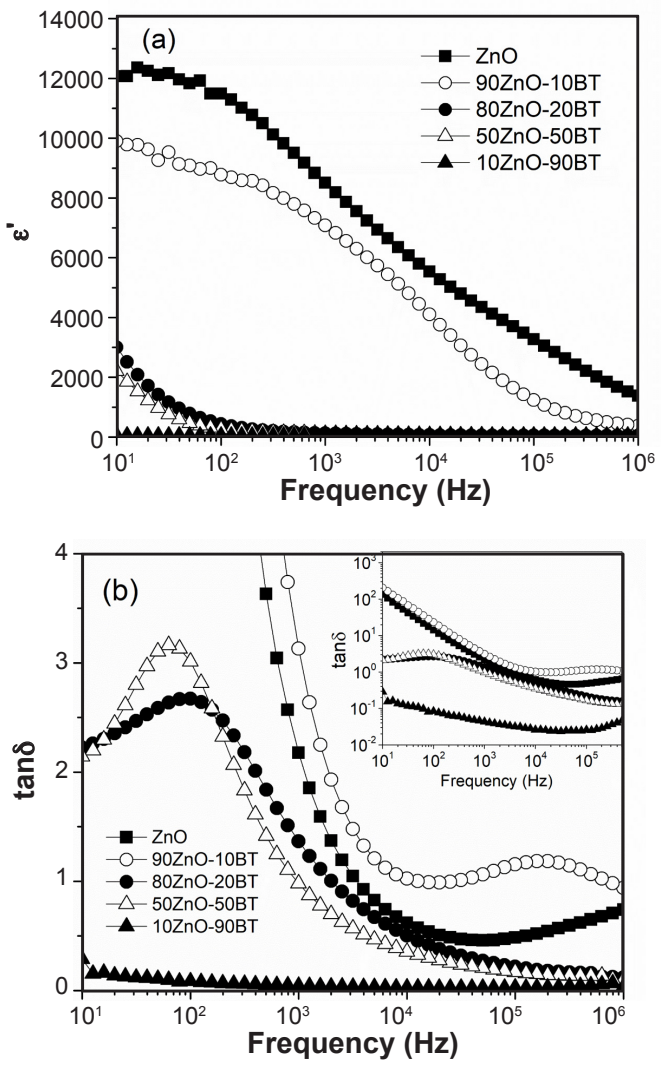

Figure 5: Room temperature dielectric properties of ZnO-BT composites over a frequency range from 10 Hz to 1 MHz: a) dielectric constant (ε'); and b) dielectric loss (tanδ).

behavior became evident for 80ZnO-20BT and 50ZnO-50BT. The presence of high capacitance associated with high dielectric loss at low frequencies is related to Maxwell-Wagner polarization [28]. In particular, dielectrics loss peaks are resolved for 80ZnO-20BT and 50ZnO-50BT. These loss peaks should not be associated with any phase transition and reinforce the statement of the Maxwell-Wagner polarization [29]. We presented the dielectric loss also on a logarithmic scale for better visualization (insert in Fig. 5b). It is interesting to observe that the low densities composites of 10ZnO-90BT presented the lowest dielectric loss and permittivity. Besides, the pure ZnO showed, together with the 90ZnO-10BT, the highest values of permittivity and dielectric loss.

The porosity in electroceramics deteriorates the permittivity, increases the dielectric loss, and decreases the dielectric strength [18]. As observed, the introduction of high quantities of BT in ZnO ceramics resulted in high porosity and we had difficulty in comparing the dielectric properties of the composites. One way to estimate the permittivity of porous ceramics is by applying the Wiener equation that is frequently used for ceramics with moderate porosities [30]:

$$\varepsilon' \cong \varepsilon^{PF}\left(1 - \frac{3}{2}V\right) \quad (B)$$

where ε^{PF} and ε' are the permittivity values of porous free and porous materials, respectively. The porosity (V) can be calculated by:

$$\rho^{P} = \rho_{theo}\,(1\text{-}V) \quad (C)$$

where ρ^{P} and ρ_{theo} are the density values for porous ceramic and calculated by crystallographic data (theoretical), respectively. To perform a direct comparison between the samples, we calculated the ε^{PF} of ZnO-BT ceramics (Table I). Accordingly, the correction of porosity did not change the observed reduction of permittivity with BT content. This observation applies even for the composition 90ZnO-10BT, which presented low porosity. Once BT is a ferroelectric ceramic with a high dielectric constant, the inverse of this trend was expected. The literature for BT ceramics sintered by low-temperature techniques reports typically low permittivity values at room temperature (~600) [3, 15]. This value is several times lower than the permittivity measured for ZnO and 10ZnO-90BT and higher than that measured for 80ZnO-20BT, 50ZnO-50BT, and 10ZnO-90BT.

The permittivity and resistivity are, by definition, independent quantities. However, due to dispersive transport and interfacial polarization, they are frequently inter-related. Accordingly, composites and polycrystalline materials may present interfacial polarization and the conduction leads to dielectric losses that influence the permittivity. Ceramics of BT and ZnO present different resistivities and permittivities and we expected that ZnO would provide space charges that accumulate at interfaces of BT and ZnO [31]. Besides, the dielectric responses of grains are dominant at high frequencies, while grain boundaries are dominant at low frequencies. This observation can explain the dielectric loss peak observed for 80ZnO-20BT and 50ZnO-50BT composites (Fig. 5). However, it does not explain the high ε' and $\tan\delta$ for ZnO and 90ZnO-10BT. To advance this discussion, note in Table I and Fig. 5 that the increase in BT content to values greater than 10 wt% decreased the dielectric loss and the permittivity while increased the resistivity. It has been shown that the CSP influences the compositional and structural characteristics of ZnO grain boundaries [26], which could increase the interfacial polarization processes. This process increases the permittivity and the dielectric loss of the composites. The increase in BT content to higher values seems to degrade this mechanism, most likely due to the increase in porosity and the lack of interconnectivity between the grains. In other words, the high permittivities values of pure ZnO and ZnO with low contents of BT are due to the interfacial polarization at room temperature.

CONCLUSIONS

Ceramics of ZnO and composites of ZnO-BT were sintered at 250 °C/1 h. High densities (>95%) were obtained for pure ZnO and ZnO with 10 wt% of $BaTiO_3$ (BT). The increase of BT content reduced the grain size of the composite while reduced the sinterability. The low treatment temperatures used in the cold sintering process prevented the diffusion between the phases. This paper identified that BT addition to ZnO increases the resistivity of composites while reduces dielectric loss and permittivity.

ACKNOWLEDGMENTS

This work was supported by CNPq (Grant # 2014/456879-5) and FAPESP (Grant # 2011/08497-6), two Brazilian research-funding agencies.

REFERENCES

[1] N.J. Shaw, Powder Metall. **21**, 6 (1989) 25.
[2] H. Guo, A. Baker, J. Guo, C.A. Randall, J. Am. Ceram. Soc. **99**, 11 (2016) 3489.
[3] L. Karacasulu, M. Tokkan, M. Bortolotti, G. Ischia, U. Adem, C. Vakifahmetoglu, Ceram. Int. **46**, 10 (2020) 16670.
[4] S. Grasso, M. Biesuz, L. Zoli, G. Taveri, A.I. Duff, D. Ke, A. Jiang, M.J. Reece, Adv. Appl. Ceram. **119**, 3 (2020) 115.
[5] S.K. Lee, K.Y. Mun, Y.H. Kim, J. Lhee, T. Okuchi, J.F. Lin, J. Phys. Chem. Lett. **11**, 8 (2020) 2917.
[6] C. Vakifahmetoglu, L. Karacasulu, Curr. Opin. Solid State Mater. Sci. **24**, 1 (2020) 100807.
[7] J.P. Maria, X. Kang, R.D. Floyd, E.C. Dickey, J. Mater. Res. **32**, 17 (2017) 3205.
[8] A. Baker, H. Guo, J. Guo, C. Randall, J. Am. Ceram. Soc. **99**, 10 (2016) 3202.
[9] D. Wang, H. Guo, C.S. Morandi, C.A. Randall, S. Trolier-McKinstry, APL Mater. **6**, 1 (2018) 16101.
[10] S. Funahashi, J. Guo, H. Guo, K. Wang, A.L. Baker, K.

Shiratsuyu, C.A. Randall, J. Am. Ceram. Soc. **100**, 2 (2017) 546.
[11] H. Guo, J. Guo, A. Baker, C.A. Randall, ACS Appl. Mater. Interfaces **8**, 32 (2016) 20909.
[12] J. Gonzalez-Julian, K. Neuhaus, M. Bernemann, J.P. da Silva, A. Laptev, M. Bram, O. Guillon, Acta Mater. **144**, 1 (2018) 116.
[13] H. Guo, A. Baker, J. Guo, C.A. Randall, ACS Nano **10**, 11 (2016) 10606.
[14] J.P. Ma, X.M. Chen, W.Q. Ouyang, J. Wang, H. Li, J.L. Fang, Ceram. Int. **44**, 4 (2018) 4436.
[15] K. Tsuji, A. Ndayishimiye, S. Lowum, R. Floyd, K. Wang, M. Wetherington, J.P. Maria, C.A. Randall, J. Eur. Ceram. Soc. **40**, 4 (2020) 1280.
[16] J. Guo, X. Zhao, T.H. De Beauvoir, J.H. Seo, S.S. Berbano, A.L. Baker, C. Azina, C.A. Randall, Adv. Funct. Mater. **28**, 39 (2018) 1.
[17] A.G. Serrano, A.L. Bonaventura, R. Boschilia, E. Antonelli, Mater. Res. Bull. **87**, 1 (2017) 34.
[18] A.C. Caballero, J.F. Fernández, C. Moure, P. Durán, J. Eur. Ceram. Soc. **17**, 4 (1997) 513.
[19] A.C. Caballero, J.F. Fernández, C. Moure, P. Durán, Y.M. Chiang, J. Am. Ceram. Soc. **81**, 4 (1998) 939.
[20] X. Wang, P. Ren, J. Wang, J. Xu, Y. Xi, J. Eur. Ceram. Soc. **40**, 5 (2020) 1896.
[21] Y. Slimani, A. Selmi, E. Hannachi, M.A. Almessiere, A. Baykal, I. Ercan, J. Mater. Sci. Mater. Electron. **30**, 10 (2019) 9520.
[22] H. Kundalia, B. Vyas, C. Savaliya, M. Udeshi, S. Jethva, S. Katba, P. Trivedi, D. Kuberkar, AIP Conf. Proc. **1837**, 1 (2017) 4.
[23] R.J. Magyar, S. Root, T.R. Mattsson, J. Phys. Conf. Ser. **500**, 16 (2014) 162004.
[24] ASTM E1382, "Standard test methods for determining average grain size using semiautomatic and automatic image analysis", Am. Soc. Test. Mater. (1991).
[25] A.K. Jonscher, Nature **267**, 1 (1977) 673.
[26] Y. Jing, N. Luo, S. Wu, K. Han, X. Wang, L. Miao, Y. Wei, Ceram. Int. **44**, 16 (2018) 20570.
[27] J. Wong, J. Appl. Phys. **51**, 8 (1980) 4453.
[28] L.M. Nunes, E. Antonelli, M.I.B. Bernardi, T.O. Oladeinde, J.A.S. Caceres, J.C. M'Peko, Mater. Res. Bull. **46**, 1 (2011) 136.
[29] E. Antonelli, J.C. M'Peko, A.C. Hernandes, Phys. Status Solidi B Basic Res. **244**, 9 (2007) 3390.
[30] D.F. Rushman, M.A. Strivens, Proc. Phys. Soc. **59**, 6 (1947) 1011.
[31] Y. Slimani, A. Selmi, E. Hannachi, M.A. Almessiere, A. Baykal, I. Ercan, J. Mater. Sci. Mater. Electron. **30**, 10 (2019) 9520.
(Rec. 28/07/2020, Rev. 15/09/2020, Ac. 21/09/2020)